J Mater Sci (2009) 44:5773–5780
DOI 10.1007/s10853-009-3809-9

High temperature flexural strength and fracture toughness of AlN with Y_2O_3 ceramic

Humberto N. Yoshimura · Nilson E. Narita · André L. Molisani · Hélio Goldenstein

Received: 16 March 2009 / Accepted: 13 August 2009 / Published online: 26 August 2009

Abstract The effects of temperature on the fast fracture behavior of aluminum nitride with 5 wt% Y_2O_3 ceramic were investigated. Four-point flexural strength and fracture toughness were measured in air at several temperatures (30–1,300 °C). The flexural strength gradually decreased with the increase of temperature up to 1,000 °C due to the change in the fracture mode from transgranular to intergranular, and then became almost constant up to 1,300 °C. Two main flaw types as fracture origin were identified: small surface flaw and large pores. The volume fraction of the large pores was only 0.01%; however, they limited the strength on about 50% of the specimens. The fracture toughness decreased slightly up to 800 °C controlled by the elastic modulus change, and then decreased significantly at 1,000 °C due to the decrease in the grain-boundary toughness. Above 1,000 °C, the fracture toughness increased significantly, and at 1,300 °C, its value was close to that measured at room temperature.

Introduction

Aluminum nitride (AlN) ceramics have been used as electronic package material for high power devices mainly because of their high thermal conductivity [1, 2]. They have been produced by a pressureless liquid-phase sintering process with aluminate-forming additives, like Y_2O_3 and CaO [3, 4]. AlN has potential to be applied as structural material since its mechanical strength is close to that of alumina.

From the Griffith–Irwin fracture criterion, the flexural strength, σ_f, and fracture toughness, K_{Ic}, are related by [5, 6]:

$$\sigma_f = \frac{K_{Ic}}{Y\sqrt{C}}, \quad (1)$$

where Y is a geometrical constant and C the size of the defect that initiate the fracture. Some works investigated the mechanical behavior of AlN at room temperature. Abe et al. [7] concluded that large intra and intergranular pores in pressed green bodies limited σ_f in an AlN with 5 mol% Y_2O_3 ($\sim$300–340 MPa). Watari et al. [8] could prepare AlN with high σ_f (450 MPa) by sintering it at low temperature with the aid of Y_2O_3, CaO, and Li_2O additives. Terao et al. [9] observed that the addition of La_2O_3 or Sm_2O_3, replacing Y_2O_3, increased the values of σ_f and K_{Ic} of AlN ceramics. Using a stochastic model based on the fracture path, they concluded that the increase in strength was caused by the increase in both the fracture toughness of grain boundaries and the fracture toughness of AlN grains [9]. Similarly, it has been attributed that additions of CaO decrease the mechanical properties (σ_f and K_{Ic}) of AlN because the fracture path changes to intergranular mode [10].

At high temperature, the mechanical behavior of AlN ceramics is usually investigated in inert environments. For a hot-pressed pure AlN tested at 1,027 °C in nitrogen atmosphere, De With and Hattu [11] observed that σ_f diminished 21% while K_{Ic} increased 15% in relation to the values measured at room temperature. Li and Watanabe [12] investigated a pressureless sintered AlN with 2 vol.% Y_2O_3 in argon atmosphere and also observed a decrease of

H. N. Yoshimura (✉)
Federal University of ABC, Rua Santa Adélia, 166, Santo André, SP 09210-170, Brazil
e-mail: humberto.yoshimura@ufabc.edu.br

N. E. Narita · A. L. Molisani · H. Goldenstein
Polytechnic School of the University of São Paulo, Av. Prof. Mello Moraes, 2463, São Paulo, SP 05508-900, Brazil

40% in σ_f between room temperature and 1,500 °C. In creep studies [13–16], AlN ceramics have shown intergranular deformation controlled by diffusional creep, formation of dislocation network, and cavitation in grain boundaries.

It has been observed that AlN with Y_2O_3 substrates oxidize in air above 800 or 900 °C [17, 18]. The oxidation layer formed at the surface may decrease the flexural strength of AlN substrates at room temperature, since the thermal expansion mismatch between AlN and Al_2O_3 may introduce severe cracking in this layer [18]. For a hot-pressed pure AlN, the flexural strength measured in air decreased 37% with the increase of testing temperature from room temperature to 800 °C and then remained almost constant up to 1,300 °C [19].

As shown, there are only few works that investigated the high temperature mechanical properties of sintered AlN ceramics. For application of AlN as structural material, it is important to know the mechanical behavior in oxidizing environments. In this work, the values of flexural strength and fracture toughness of an AlN with 5 wt% Y_2O_3 were measured in air between room temperature and 1,300 °C. Using fractographic analysis, the defects that limited the strength could be identified and the fracture mode could be correlated to the variation of mechanical properties.

Experimental

AlN powder (grade C, Stark) and 5 wt% Y_2O_3 powder (grade C, Stark) were ball-milled for 24 h in a plastic-coated jar, using high-purity alumina balls and isopropyl alcohol as milling medium to avoid the hydrolysis of the AlN powder. A binder (polyethylene glycol, 2 wt%) was added to the suspension in the last hour of milling. The suspension was dried in a rotoevaporator and the powder was granulated using an 80 mesh nylon screen. The granulated powder was first uniaxially pressed in a steel mold with cavity area of 50 × 70 mm at 20 MPa and then isostatically pressed at 190 MPa. The green plates were vertically placed on a bed of AlN powder inside a graphite crucible internally covered with a BN coating. This procedure was adopted to avoid an excessive reducing atmosphere (CO gas) near the green plates, which can cause evaporation of additives and inhibition of densification [20]. The plates were pressureless sintered at 1,820 °C for 1 h, after a debinding step at 500 °C for 1 h, in a graphite heated furnace (1000-4560-FP20, Thermal Technology) using a high-purity N_2 gas flow (2 L/min). The heating and cooling rates were 10 and 30 °C/min, respectively. The surfaces of sintered plates (dimensions of 58 × 38 × 7 mm^3) were machined and then the plates were sliced to prepare bar specimens. The specimens were then machined to dimensions of 3 × 4 × 58 mm^3 in accordance to the recommendations of ASTM C-1211 standard. For bending test, the surface loaded in tension was polished with varying diamond grits (from 15–0.25 μm). The corners of the bar specimens were beveled to remove edge chipping.

The flexural strength was measured at room temperature, 800, 1,000, 1,200, and 1,300 °C in air using a fully articulated four-point bending fixture (SiC) with 20 and 40 mm spans. A testing machine (Syntech 5/G, MTS) was used in the bending tests and the crosshead speed was 0.5 mm/min. For high temperature tests, a $MoSi_2$ heated furnace was used. The heating rate was 30 °C/min up to the temperature 100 °C below the testing temperature, and the final heating rate was 5 °C/min. The specimen was soaked at the testing temperature for 6 min before loading. A preload of 5 N was applied to the specimens to avoid the displacement of supporting rollers during the heating cycle.

The fracture toughness was determined using the surface crack in flexure (SCF) method. A controlled semi-elliptical surface flaw was introduced at the center of the tension surface using a two-step procedure. First, a Knoop indentation with a load of 71 N was impressed with its longer diagonal transversally aligned to the longer axis of bar specimen. Second, the indented surface was ground with a 1,000 grit emery paper to remove a layer of material (thickness of ~50 μm). This procedure removed the residual stress zone associated to the Knoop impression, leaving a semi-elliptical stress-free precrack at the surface.

The specimen was then tested using the four-point bending fixture with 20 and 40 mm spans to record the fracture stress, with the same testing conditions used for flexural strength measurement. The width and depth of semi-elliptical surface flaw were measured on both fractured surfaces using an optical microscope (DMRXE, Leica) and a scanning electron microscope (JMS 6300, Jeol). The value of fracture toughness, K_{Ic}, was calculated using the equations proposed in ASTM C-1421 standard. The fracture toughness at high temperature (800, 1,000, 1,200, and 1,300 °C) was also determined in air, using the same heating cycle used for flexural strength measurement at high temperature.

The Young's modulus at room temperature was determined by the pulse-echo method using a pulser-receiver of 200 MHz (5900 PR, Panametrics) and the bulk density was determined by Archimedes method. The crystalline second-phase was identified by X-ray diffraction analysis (Rint 2000, Rigaku) and the microstructural and fractographic analyses were performed using optical microscopy, scanning electron microscopy (SEM), and energy dispersive spectroscopy (EDS, Noram) coupled to the SEM. The size of the defect that limited the flexural strength was calculated as geometric average of the long and short axis assuming an elliptical or semi-elliptical shape [21].

The results in the text are shown as average ± one standard deviation in the mean. Four to six specimens for each mechanical testing condition were evaluated. The statistical analysis of the results used Student's *t*-test method at 90% confidence interval. The SEM images shown in the next section are secondary electron images, except when another type (backscattered electron image) is indicated.

Results and discussion

The bulk density of pressureless sintered AlN with 5 wt% Y_2O_3 specimens was 3.33 ± 0.01 Mg/m^3 (99.6% of the theoretical density). The microstructure of this material had isometric AlN grains (grain size of ~5 μm), second-phase particles of YAG ($3Y_2O_3{\cdot}5Al_2O_3$) at the grain boundaries, and few residual pores (Fig. 1). In Fig. 1, the secondary electron image shows two different gray colors in the AlN matrix, but the reason for this contrast could not be accessed since the backscattered electron images did not show any contrast and EDS analysis detected only Al and N in different regions of the AlN matrix.

Flexural strength

The results of the four-point flexural strength ($\sigma_{f,4}$) measurements in air at several temperatures are shown in Table 1. The strength decreased with the increase of testing temperature up to 1,000 °C. The reduction at 800 °C was almost 15% in relation to the value measured at room temperature (277 MPa). Between 1,000 and 1,300 °C, the strength stabilized at around 220 MPa (a reduction of ~20% with respect to the room temperature value). This trend was similar to that observed for the hot-pressed pure AlN tested in air [19].

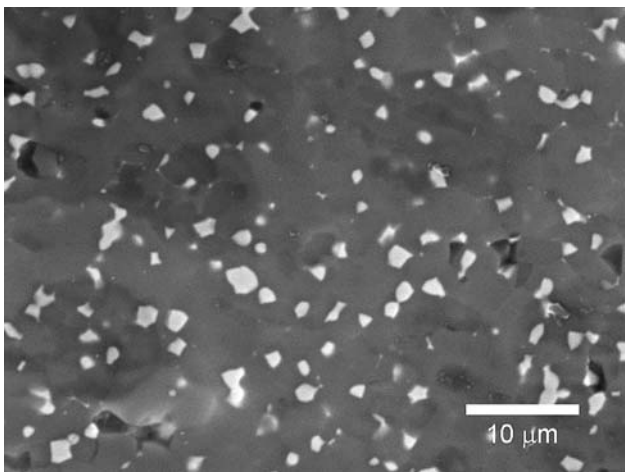

Fig. 1 SEM micrograph of AlN with 5 wt% Y_2O_3 sintered at 1,820 °C. EDS analysis detected N and Al in the dark grains and O, Al, and Y in the light particles, which were identified by XRD analysis as AlN and YAG ($3Y_2O_3{\cdot}5Al_2O_3$) phases, respectively

Table 1 Results of four-point flexural strength ($\sigma_{f,4}$) and fracture toughness (K_{Ic}) measured in air as a function of testing temperature

T (°C)	$\sigma_{f,4}$ (MPa)	K_{Ic} (MPa m$^{1/2}$)
30	277 ± 38[a]	2.98 ± 0.11[a]
800	236 ± 34[a,b]	2.91 ± 0.17[a,b]
1,000	226 ± 47[b]	2.50 ± 0.06[b]
1,200	220 ± 35[b]	2.88 ± 0.11[a]
1,300	226 ± 15[b]	2.99 ± 0.06[a]

The results of each column followed by the same letter are not statistically different at 90% confidence interval

Fractographic analysis showed two types of defects as fracture origin, irrespective of the testing temperature. The first type was a semi-elliptical surface flaw with dimensions of up to 100 μm (Fig. 2a). These defects were probably introduced during the machining or polishing steps, even though a careful procedure was adopted to minimize the occurrence of surface damages. The image shown in Fig. 2a was taken from an area inside the mirror region, and the hackle lines surrounding this region were observed at lower magnifications confirming that the indicated surface flaw was the fracture origin that limited the flexural strength. The second type consisted of large pores with dimensions ranging from ~100 to 200 μm (Fig. 2b). The size and shape of these pores indicated that they were processing defects, possibly organic inclusions introduced during the powder preparation, which was burned out during the heating stage of sintering cycle. In fact, the analysis of green bodies showed the presence of large carbon-rich particles (Fig. 3a). In some cases, around the large pores in sintered specimens, regions depleted of second-phase particles were observed (Fig. 3b). This probably occurred because a reducing CO gas, formed by the reaction between the organic inclusion and the oxides (Y_2O_3 additive and Al_2O_3 from surface of AlN particles), caused the local evaporation of the second phase [20]. The source of the powder contamination is not clear yet, but it seems that the nylon screen used to granulate the powder was the source. Hereinafter, the first type of defects will be referred as surface defect and the second type as volume defect (Fig. 2).

In Fig. 4, the values of the fracture stress of all specimens are plotted with the identification of the type of fracture origin, surface (*S*), or volume (*V*) defect. In general, higher fracture stresses were observed in specimens fractured from surface defects. At room temperature, the four-point flexural strength ($\sigma_{f,4}$), considering only the specimens fractured from surface defects, was 305 MPa, while considering only volume defects the strength was

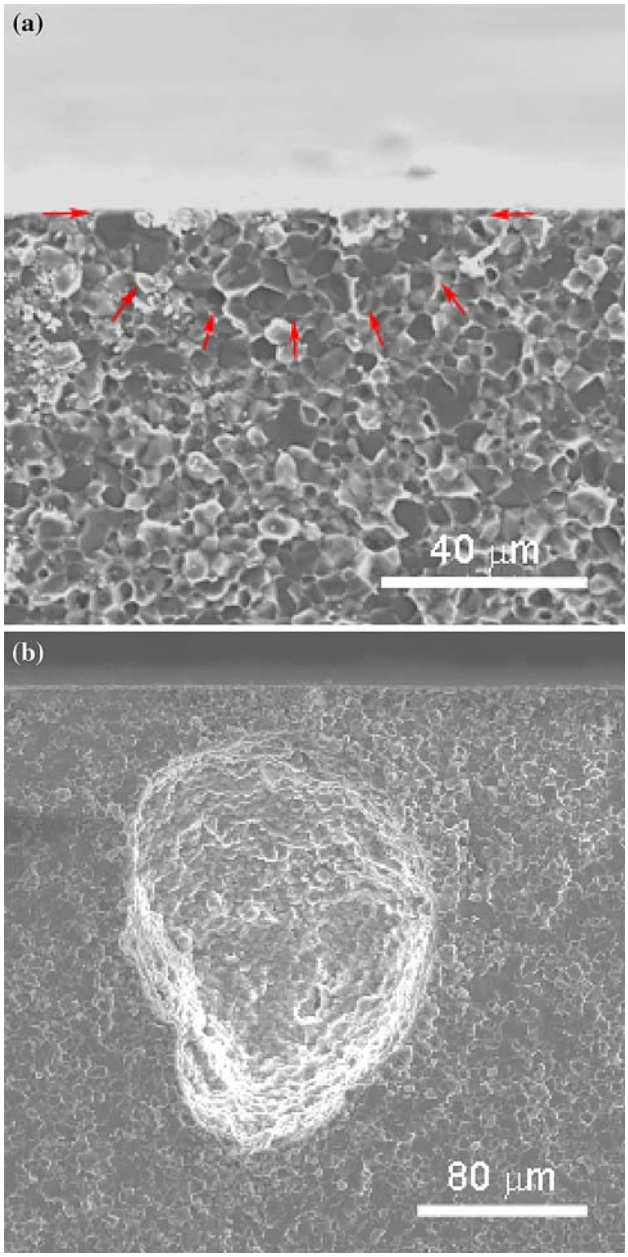

Fig. 2 SEM images of fracture origins: **a** semi-elliptical surface flaw (surface defect); and **b** large pore (volume defect)

248 MPa. These results showed that the large pores (Fig. 2b) reduced the material's strength by 19%. Although the surface defects are in principle more deleterious to mechanical strength than volume defects [6], the size of large pores made the volume defects in this case more severe. The microstructural analysis showed only a few large pores on the polished surface of bending bars and the measured volume fraction of these pores was only 0.01%. These large pores, however, limited the strength of around 50% of the tested specimens (Fig. 4). These results show that AlN ceramics are sensitive to large processing defects,

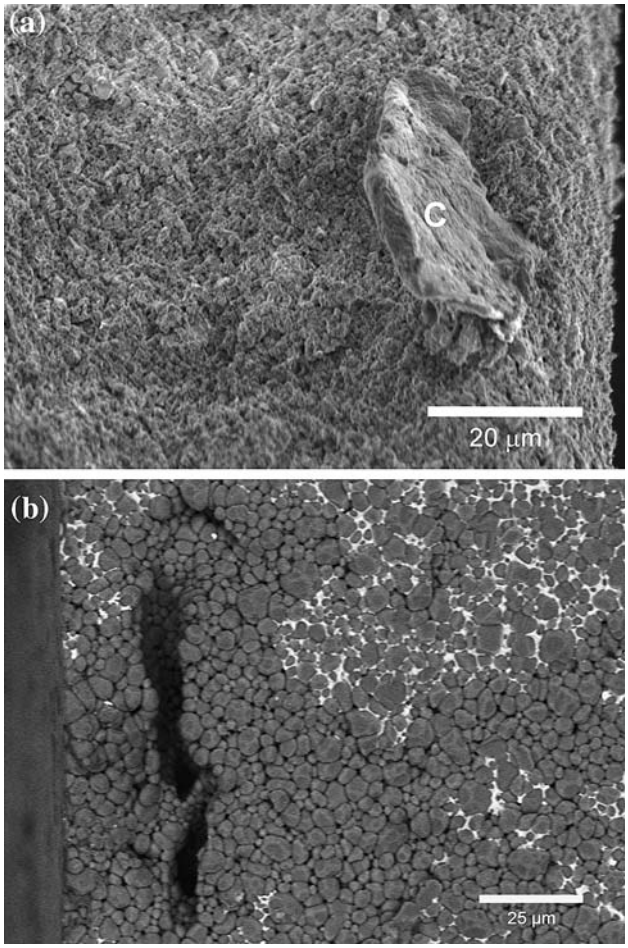

Fig. 3 SEM images of: **a** a carbon-rich inclusion (*indicated with letter C*) in an AlN green body (confirmed by EDS analysis); and **b** backscattered electron image showing a large pore in a sintered body probably caused by the decomposition of an organic inclusion and a region around the pore depleted of YAG phase (*light areas*)

as has been observed in other ceramics, like Al_2O_3 and Si_3N_4 [22, 23].

Figure 5 shows SEM images of polished surfaces of the specimens exposed at high temperatures in oxidizing atmosphere (air) during the thermal cycle of the bending test. The microstructure of the surfaces heated to 800 and 1,000 °C (Fig. 5a) did not show any change, like the formation of oxidation layers or the occurrence of surface attacks, and its characteristics were similar to the initial surface (Fig. 1). The EDS analysis of the exposed surface, however, detected a small fraction of oxygen, indicating that the oxygen diffused into the material even at 800 °C. The surface of specimens heated to 1,200 °C was slightly attacked, highlighting the AlN grain structure. At 1,300 °C, the oxidation was more severe and the specimen's surface was rougher than at 1,200 °C, but no oxidation layer could be observed (Fig. 5b). The EDS analysis indicated an increase in oxygen content on the polished surface with the

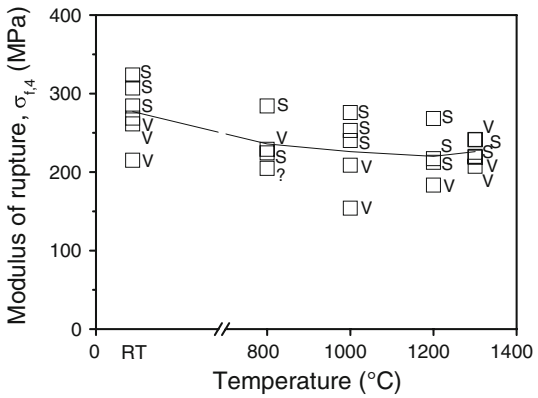

Fig. 4 Four-point flexural strength ($\sigma_{f,4}$) as a function of testing temperature. *S* and *V* indicate the type of fracture origin: surface or volume defect, respectively. *Full line* shows the tendency of variation of average values

increase of testing temperature. However, the oxidation of AlN surface did not influence the flexure strength between 1,000 and 1,300 °C (Fig. 4).

Fracture surface micrographs of the specimens tested at different temperatures are shown in Fig. 6. Specimens tested at room temperature showed predominantly transgranular fracture (Fig. 6a). The increase of the testing temperature to 800 °C increased the occurrence of intergranular fracture, but the fracture path was predominantly transgranular (Fig. 6b). At higher temperatures (≥1,000 °C), the fracture mode changed significantly, since the surfaces presented predominantly intergranular fracture (Fig. 6c, d). The results indicate that the fracture of AlN with 5 wt% Y_2O_3 was dominated by the fracture of AlN grains up to 800 °C, and above this temperature, it was controlled by fracture at the grain boundaries. The change of fracture mode from transgranular to intergranular with the increase of testing temperature was correlated with the decrease of flexural strength up to 1,000 °C (Fig. 4). The weakening of grain boundaries possibly is associated with the mechanical behavior of YAG second-phase in these boundaries. Although single-crystal YAG is one of the most creep-resistant oxides [24, 25], the strain rates are significantly higher in polycrystalline YAG [26] and sintered Al_2O_3–YAG composite, because the grain boundaries and amorphous phase at the interfaces are rapid paths to diffusion process [27]. In addition, the flexural strength of sintered Al_2O_3–YAG composites decreased rapidly above 800 °C, and the fracture mode was intergranular [28]. Similarly, the YAG/AlN interfaces can have contributed to the weakening of AlN grain boundaries.

Fracture toughness

The results of the fracture toughness (K_{Ic}) measurements at several temperatures in air are shown in Table 1. At the

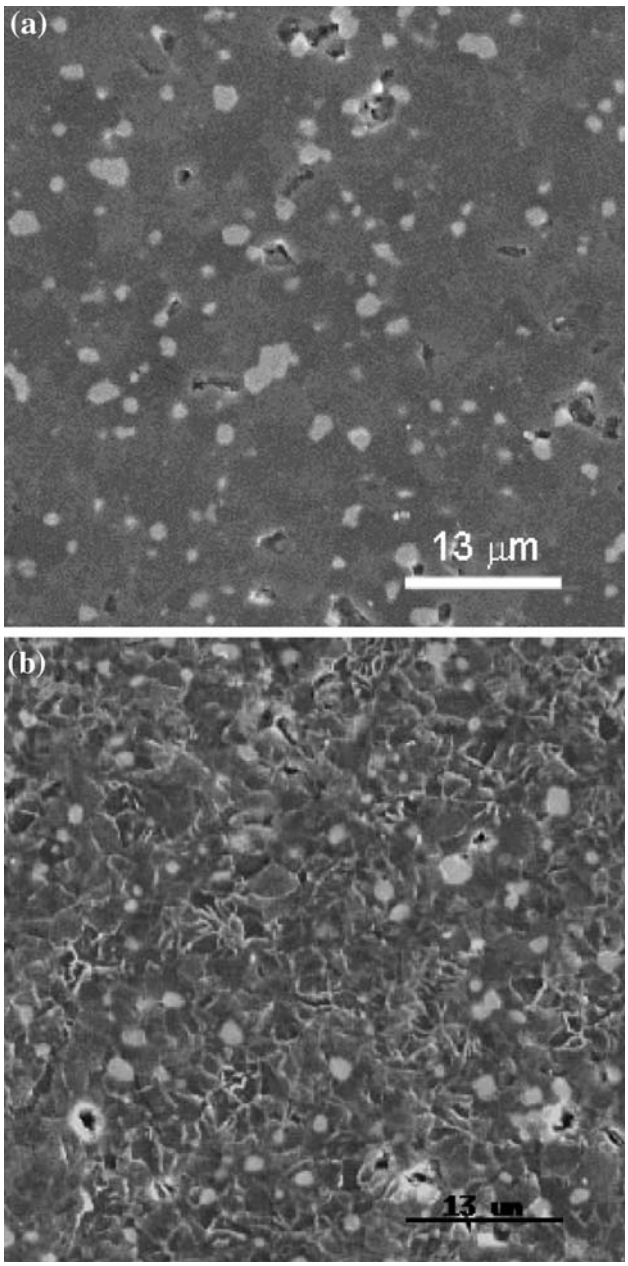

Fig. 5 SEM micrographs of the tension surface of specimens tested at: **a** 1,000 °C and **b** 1,300 °C

90% confidence interval, there was no significant difference between the values of K_{Ic} measured at room temperature and 800 °C (Table 1), but the value measured at 1,000 °C was significantly lower than the value measured at room temperature (reduction by 16%). Above 1,000 °C, K_{Ic} increased significantly with the increase of testing temperature up to 1,300 °C. For this temperature, the average value of K_{Ic} was close to that measured at room temperature (2.98 ± 0.11 MPa $m^{1/2}$). Abe et al. [7] reported a similar result (2.9 MPa $m^{1/2}$) for an AlN with 5 wt% Y_2O_3 tested by the SCF method at room temperature.

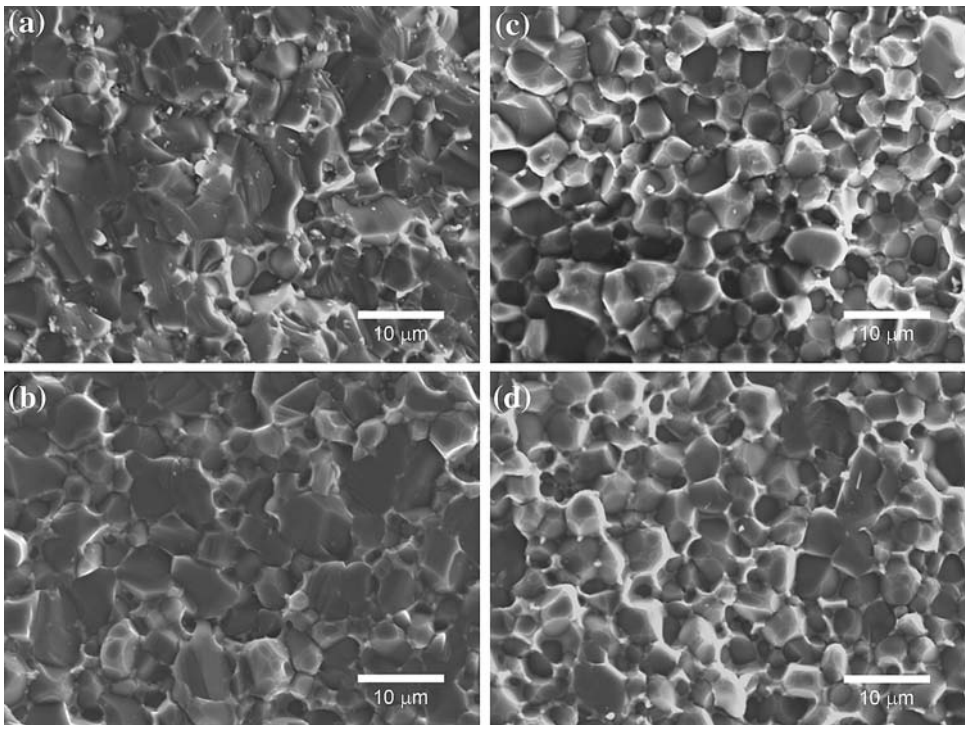

Fig. 6 SEM micrographs showing the fracture path of specimens broken in flexural test at different temperatures: **a** room temperature; **b** 800 °C; **c** 1,000 °C; and **d** 1,300 °C

Stewart and Bradt [29] proposed an equation for the decrease of K_{Ic} with the increase of temperature based on the decay of elastic modulus:

$$\frac{dK_{Ic}}{dT} = \frac{\lambda\sqrt{2}}{\pi a_0^{1/2}(1-\nu^2)^{1/2}}\left[\left(\frac{dE}{dT}\right) - \frac{1}{2}(E\alpha) - \frac{E\nu}{1-\nu^2}\left(\frac{d\nu}{dT}\right)\right], \quad (2)$$

where λ is the relaxation distance of ion forces, a_0 the interatomic distance, ν the Poisson's ratio, E the Young's modulus, and α the linear thermal expansion coefficient. Considering $\alpha = 5.6 \times 10^{-6}$ °C^{-1} [30], data of dE/dT for AlN with 4 wt% Y_2O_3 from Bruls et al. [31], $d\nu/dT = 0$ [29], and calculating the term $\lambda\sqrt{2}/\pi a_0^{1/2}(1-\nu^2)^{1/2}$ using the measured values of K_{Ic} and E at room temperature, the predicted decay of K_{Ic} with temperature from Eq. 2 could be calculated, and it is plotted in Fig. 7 together with the experimental data.

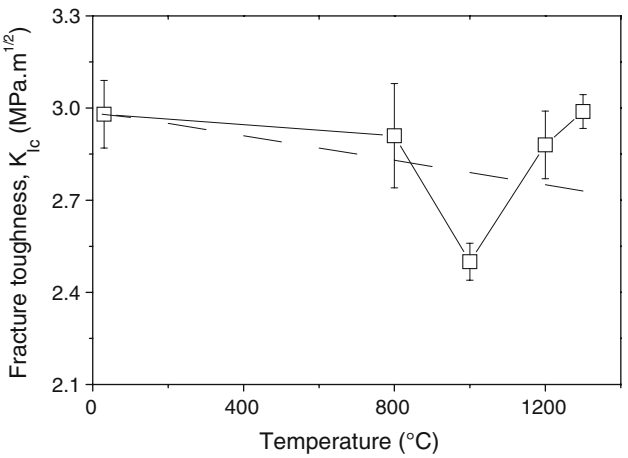

Fig. 7 Fracture toughness (K_{Ic}) as a function of testing temperature. The *dotted line* is the curve predicted from Eq. 2

The measured value of K_{Ic} at 800 °C is in good agreement with that predicted by the model proposed by Stewart and Bradt [29]. Therefore, the slight decrease in K_{Ic} at 800 °C can be attributed to the decrease in Young's modulus of AlN. The predominance of transgranular fracture mode at this temperature (Fig. 6b) reinforces this explanation [29]. This means that the fracture toughness of the AlN grains controlled the overall K_{Ic} of material [9, 32]. The rapid decrease of K_{Ic} above 800 °C seems to be related to the fracture mode change from transgranular to intergranular. The fracture path was predominantly intergranular at 1,000 °C (Fig. 6c) indicating that K_{Ic} was affected by the mechanical behavior of YAG second-phase at grain boundaries or YAG/AlN grain interfaces, which means that the material's K_{Ic} was controlled by the fracture toughness of grain boundary [9, 32]. A spinel ($MgAl_2O_4$) ceramic also showed an abrupt change of the decay rate of K_{Ic} with temperature, when the fracture path changed from a mixed (inter and transgranular) mode to a complete intergranular fracture mode [29]. This rapid decrease of K_{Ic} with increase in temperature, above the fracture mode transition temperature, was attributed to an operation of inelastic mechanisms at high temperature [29]. Stewart and Bradt [29] refuted the possible grain size dependent

mechanisms, such as loss of grain-boundary coherence and crack-tip plasticity-enhanced crack propagation, since K_{Ic} was not influenced by the grain size.

The reason for the increase in K_{Ic} above 1,000 °C is not clear. This increase could explain the maintenance of the flexural strength between 1,000 and 1,300 °C (Fig. 4), counteracting the weakening of grain boundaries. In case of brittle fracture, the measured mechanical properties must follow the Griffith–Irwin relation (Eq. 1). Using this equation (considering $Y = 1.24$) [21] and the measured values of flexural strength and fracture toughness (Table 1), the critical flaw size was calculated and then compared with the values measured by fractographic analysis (Fig. 8). The calculated values were fairly close to the measured values for the specimens tested at 1,000 °C, validating the K_{Ic} measured at this temperature, and discarding the possible operation of an inelastic mechanism, which could have lead to invalidate the Griffith–Irwin relation (Eq. 1). This result reinforces the rationale that the material's K_{Ic} at 1,000 °C was controlled by the fracture toughness of the grain boundaries. However, the calculated values of the flaw size were higher than the measured values for specimens tested at 1,300 °C (Fig. 8), indicating that the value of K_{Ic} measured at this temperature was overestimated.

The precrack introduced by SCF method was clearly identified in all specimens tested. There was no significant difference between the precrack surfaces of the specimens tested at 1,000 and 1,300 °C, which could explain the increase of K_{Ic} value in this temperature range. Also, no halo, indicative of the occurrence of slow crack growth, was observed around the precrack front, excluding the necessity to introduce corrections on the precrack dimensions [33, 34]. Significant effects of air oxidation on the surfaces of specimens tested above 1,000 °C (Fig. 5b) suggested that oxidation may have affected the precrack characteristics of the specimens tested at 1,200 and 1,300 °C. In addition, as Li and Watanabe [12] observed a continuous decrease in flexural strength with the increase of temperature in an AlN with 2 vol.% Y_2O_3 tested in argon atmosphere, surface oxidation seems to have influenced the arresting of flexural strength with the increase in temperature. A careful SEM analysis on the crack tips and crack wakes, however, did not show any evidence of the occurrence of crack-tip blunting, microcreep, or bridging ligaments, which could have resulted in crack healing. Therefore, it was not possible to identify the toughening mechanisms which have operated above 1,000 °C. Further work involving, for example, time-dependent loading experiments and testing in different atmospheres, which are beyond the scope of this work, is needed to clarify this issue.

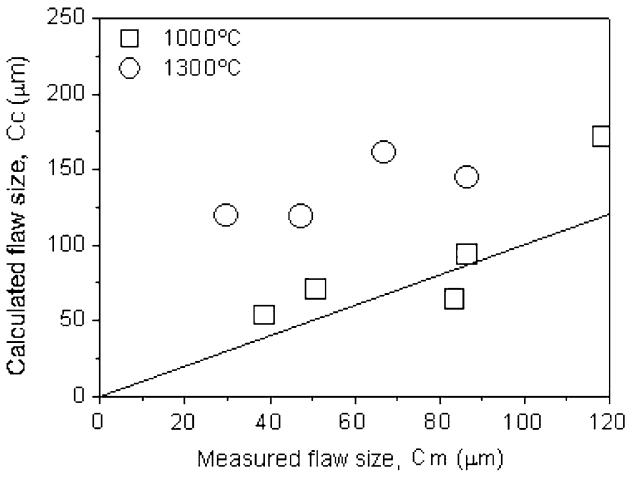

Fig. 8 Calculated flaw size (Cc) versus measured flaw size (Cm). The *full line* represents Cc = Cm

Conclusions

The mechanical testing in air and fractographic analysis of the pressureless sintered AlN with 5 wt% Y_2O_3 showed the following:

(i) The fracture toughness, K_{Ic}, slightly decreased from room temperature to 800 °C following the decay of Young's modulus. The predominance of transgranular fracture mode in this temperature range supports that the material's K_{Ic} was controlled by the fracture toughness of AlN grains. At 1,000 °C, K_{Ic} decreased significantly because of the weakening of second phase or YAG/AlN interface, changing the fracture mode to intergranular. The material's K_{Ic} at this temperature was controlled by the fracture toughness of the grain boundaries. Above 1,000 °C, K_{Ic} increased significantly and at 1,300 °C its value was close to that measured at room temperature.

(ii) The flexural strength, $\sigma_{f,4}$, decreased up to 1,000 °C, because of the decrease of K_{Ic}, then remained almost constant up to 1,300 °C, possibly because an oxidation related mechanism counterbalanced the grain-boundary weakening.

(iii) The mechanical strength of AlN with 5 wt% Y_2O_3 was sensitive to small fraction (0.01 vol.%) of large pores caused by the organic inclusions introduced during ceramic processing.

Acknowledgements The authors acknowledge the Brazilian agencies FAPESP (The State of São Paulo Research Foundation) and CNPq (The National Council for Scientific and Technological Development) for the financial support of the present research.

References

1. Ura M (1988) In: Saito S (ed) Fine ceramics. Elsevier, Tokyo
2. Streetman BG (1990) Solid state eletronic devices, 3rd edn. Prentice-Hall, New Jersey
3. Molisani AL, Yoshimura HN, Goldenstein H, Watari K (2006) J Eur Ceram Soc 26:3431
4. Molisani AL, Yoshimura HN, Goldenstein H (2009) J Mater Sci Mater Electron 20:1
5. Yoshimura HN, Molisani AL, Narita NE, Manholetti JLA, Cavenaghi JM (2006) Mater Sci Forum 530–531:408
6. Green DJ (1998) An introduction to the mechanical properties of ceramics. Cambridge University Press, Cambridge
7. Abe H, Sato K, Naito M, Nogi K, Hotta T, Tatami J, Komeya K (2005) Powder Technol 159:155
8. Watari K, Hwang HJ, Toriyama M, Kanzaki S (1999) J Mater Res 14:1409
9. Terao R, Tatami J, Meguro T, Komeya K (2002) J Eur Ceram Soc 22:1051
10. Witek SR, Miller GA, Harmer MP (1989) J Am Ceram Soc 72: 469
11. De With G, Hattu N (1983) J Mater Sci 18:503. doi:10.1007/BF00560639
12. Li J-F, Watanabe R (1994) J Ceram Soc Jpn 102:727
13. Jou ZC, Virkar AV (1990) J Am Ceram Soc 73:1928
14. Masson I, Feiereisen JP, Michel JP, George A, Mocellin A (1994) J Eur Ceram Soc 13:355
15. Feregotto V, George A, Michel J-P (1997) Mater Sci Eng A 234–236:625
16. Azzaz M, George A (2004) Mater Sci Eng A 364:84
17. Lee JW, Radu I, Alexe M (2002) J Mater Sci Mater Electron 13:131
18. Kim H-E, Moorhead AJ (1994) J Am Ceram Soc 77:1037
19. Boch P, Glandus JC, Jarrige J, Lecompte JP, Mexmain J (1982) Ceram Int 8:34
20. Lee R-R (1991) J Am Ceram Soc 74:2242
21. Mecholsky JJ Jr (1995) Dent Mater 11:113
22. Walker WJ Jr, Reed JS, Verma SK (1999) J Am Ceram Soc 82:50
23. Abe H, Hotta T, Naito M, Shinohara N, Okumiya M, Kamiya H, Uematsu K (2001) Powder Technol 119:194
24. Blumenthal WR, Phillips DS (1996) J Am Ceram Soc 79:1047
25. Deng S (1996) J Mater Sci 31:6077. doi:10.1007/BF011522162
26. Parthasarathy TA, Mah T-I, Keller K (1992) J Am Ceram Soc 75: 1756
27. Waku Y, Nakagawa N, Wakamoto T, Ohtsubo H, Shimizu K, Kohtoku Y (1998) J Mater Sci 33:4943. doi:10.1023/A:1004486303958
28. Waku Y, Nakagawa N, Wakamoto T, Ohtsubo H, Shimizu K, Kohtoku Y (1998) J Mater Sci 33:1217. doi:10.1023/A:1004377626345
29. Stewart RL, Bradt RC (1980) J Am Ceram Soc 63:619
30. Barsoum MW (1997) Fundamentals of ceramics. McGraw-Hill, New York
31. Bruls RJ, Hintzen HT, De With G, Metselaar R (2001) J Eur Ceram Soc 21:263
32. Tatami J, Yasuda K, Matsuo Y (1997) J Mater Sci 32:2341. doi:10.1023/A:1018588620081
33. Park J-K, Yasuda K, Matsuo Y (2001) J Mater Sci 36:2335. doi:10.1023/A:1017537310557
34. Yoshimura HN, Cesar PF, Miranda WG Jr, Gonzaga CC, Okada CY, Goldenstein H (2005) J Am Ceram Soc 88:1680